3-1-2014

Horizontally Issuing Diffusion Flames Characterized by OH-PLIF and Visualizations

Joshua J. Heffernen

Carl R. Hartsfield
Air Force Institute of Technology

Mark F. Reeder
Air Force Institute of Technology

Marc D. Polanka
Air Force Institute of Technology

Recommended Citation

Heffernen, J. J., Hartsfield, C. R., Reeder, M. F., & Polanka, M. D. (2014). Horizontally issuing diffusion flames characterized by OH-PLIF and visualizations. International Journal of Spray and Combustion Dynamics, 6(1), 35–65. https://doi.org/10.1260/1756-8277.6.1.35

Horizontally issuing diffusion flames characterized by OH-PLIF and visualizations

Heffernen, J.J., Hartsfield, C.R., Reeder, M.F. and Polanka, M.D.

Air Force Institute of Technology, Wright-Patterson Air Force Base, Dayton OH (US) 45433

Corresponding author: mark.reeder@afit.edu

(Submission date: May 22, 2013; Revised Submission date: August 15, 2013; Accepted date: August 23, 2013)

ABSTRACT

Planar laser induced fluorescence and flame visualizations characterized the effect of buoyancy on the behavior of the combustion zone of diffusion jet flames which issued from horizontally-oriented tubes into ambient air. The study focused on the mixing characteristics of propane and ethylene at Reynolds numbers ranging from 300 to 1500 in the near field of the jet (up to X/D =9) and Froude numbers ranging as low as 0.36, based on cold-flow gas properties and conditions. Performing the study with a variety of fuel tube diameters enabled independent control of Froude and Reynolds numbers. The PLIF visualizations revealed the presence of the hydroxyl radical in the mixing layer for all cases. The hydroxyl concentrations were consistently higher in the upper portion of the mixing layer, indicative of more vigorous mixing in this region. The visualizations also revealed the evolution of polycyclic aromatic hydrocarbons which were initially spatially segregated from the portion of the reaction zone containing the hydroxyl radical. The polycyclic aromatic hydrocarbons initiate in fuel-rich regions nearer to the jet core than the hydroxyl radical, though the two regions eventually combine well downstream of the tube exit. Both the hydroxyl radical and the polycyclic aromatic hydrocarbons were more prominent on the upper side of the jet flame. Both propane and ethylene fuels led to qualitatively similar features of the flow field, indicating the important role played by the buoyancy-influenced fluid dynamics of the combustion products. The resulting cross sectional PLIF images were used to produce a three-dimensional representation of the reaction zone, indicating the jet spread and trajectory. The data was empirically correlated and found to collapse when based on the Froude number consistent with the density and temperature of a fully-reacted stoichiometric mixture. Complementary visualizations provided additional insight into the trajectory of the jet flame and revealed features of the reaction zone farther from the tube exit.

1. INTRODUCTION

Opportunities for improved fuel efficiency and extended range for air transportation have led turbine engine developers to seek improvements in the design of combustion systems. One example of this is described as the Ultra-Compact Combustor (UCC). The premise of the UCC design is that fuel and air are injected into a circumferential cavity within the engine generating a very strong swirl component [1]. As a result of the centripetal effects (also termed g-loading), the less dense reaction products are drawn inward while more dense reactants remain in the outside cavity. This process will lead to more complete combustion process and promote higher fuel efficiency. Since the underlying physical process for the UCC is dependent upon what can be generally framed as buoyancy effects, although driven by much greater than gravitational acceleration, it is reasonable to consider how buoyancy affects the combustion process in far simpler geometries. As is often the case for laboratory studies, this simplification leads to a considerably lower Reynolds number than that of the application. Nonetheless, it is intended that his research, focused on understanding some of the physical processes in a flame with relatively low Reynolds number, will assist in understanding of the impact of those processes which are likely present in the more realistic turbulent flow environments where buoyancy is an important factor in flame propagation.

The most commonly-used burner configurations orient a premixed or fuel jet upward, either with or without an air co-flow [2, 3]. Generally speaking, the combustion accelerates the reaction products in the same direction (upward) as the initial fuel flow. To determine the effect of buoyancy on the behavior of the flame, several researchers have investigated flames under microgravity conditions [4, 5]. By comparison, the number of studies of the combustion process resulting from a fuel jet issuing horizontally from a tube or nozzle is far lower, though there are a handful of exceptions (e.g., refs. [6, 7, 8]).

The relative dearth of literature on the subject of horizontally-oriented diffusion flames could be considered somewhat surprising because such a change in orientation is relatively simple to achieve in a laboratory experiment. However, a horizontal orientation introduces many new variables and complications, by virtue of the fact that the flame geometry departs substantially from axisymmetry. As such, parametric changes in fuel type or flow rate for a horizontally issuing orientation would lead to consequences which might be difficult to anticipate, interpret, and apply broadly. However, since the less dense reaction products would attain a velocity component normal to the initial fuel flow direction (i.e., upward vis-à-vis horizontal), there is a basic commonality with the UCC design. In the UCC, the fuel-air mixture flows circumferentially within the outer cavity while products attain a radially inward component of velocity. Therefore, a horizontally issuing diffusion flame provides an opportunity to learn about some of the fundamental aspects of buoyancy relevant to the UCC as well as other fundamental geometries, motivating the current research.

In addition to the global effect of turning the flow in the direction opposite to the gravity vector, Gore and Jian [7] observe that there is second important effect due to buoyancy on mixing and turbulence. These authors note that the buoyancy acts to destabilize the flow and generate turbulent velocities in the upper half of the jet due to

buoyancy. On the other hand, these authors state that there is a tendency to stabilize the lower portion of the flame since the density would generally increase in the direction of the gravity vector in this region. This complex behavior suggested to Gore and Jian a plausible reason for the scarcity of papers dealing with the subject. Their work, motivated by the practical applications of furnaces and safety concerns for fires resulting from fuel pipe leaks, was carried out with the purpose of establishing trajectory guidelines in terms of Reynolds number and Richardson number.

In another study, Escudier used flame visualizations and emissions measurements to investigate the relative effects of buoyancy and momentum on the flame characteristics of horizontally-issuing jet flames [9]. In more recent work, Smith, Periasamy, Baird and Gollahalli studied relative effects of buoyancy and momentum on the characteristics of horizontally oriented circular flames in a quiescent environment over a wide range of jet exit velocities [10].

Horizontally issuing buoyant jets may be characterized by Reynolds number and Froude number where the dimensionless numbers are computed using the properties and conditions of the jet [11, 12]. In a diffusion flame, the fluid properties and make-up of the mixture change dramatically in a short time, and so characterizing the flow field for analysis is very challenging. For example, a non-combusting propane jet issuing horizontally into air will gain a downward trajectory due to propane's higher density. However a reacting jet will produce products with lower density since the temperatures are elevated and the products' molecular weights are slightly lower than propane. As such the diffusion flame is expected to achieve an upward jet trajectory. By varying the fuel tube diameter in combination with the mass flow rate of the fuel, the Reynolds number and Froude numbers may be varied independently from one another, and this was a key reason for performing this set of experiments.

A reference value for Reynolds number and cold flow Froude number provides some utility in assessing the initial conditions in the flow field. Since the density field varies spatially, the most convenient approach was simply to use the initial properties of the fuel, despite the shortcomings described above. Since this research involves flow within a tube, the characteristic length is the diameter, D, and the form of the Reynolds number is given in Equation (1):

$$Re = \frac{4\rho_j Q}{\pi D \mu} \tag{1}$$

where Q is the volumetric flow rate, μ is the viscosity of the fuel, and ρ_j is the density of the fuel exiting the tube. For propane at atmospheric pressure and room temperature, the density is 1.88 kg/m^3 while the density of ethylene is 1.26 kg/m^3. The respective values for viscosity are 7.8 *10^{-6} Pa-s for propane and 9.7*10^{-6} Pa-s for ethylene. Likewise, Froude number is given as:

$$Fr = \frac{4Q}{\pi D^2 \left[gD \left| \frac{\rho_a - \rho_j}{\rho_j} \right| \right]^{1/2}} \tag{2}$$

Where ρ_a is the density of the ambient air, and g is the gravitational constant. The air density was 1.17 kg/m^3 under laboratory conditions. This use of initial fuel conditions is consistent with Kolhe and Agrawal [2], who studied a vertically issuing flame. For a given fuel, such as propane, these values provide a useful reference for assessing the relative buoyancy to inertia effects if one assumes that the density field resulting from combustion is essentially the same from one jet to another. However, an important caveat is that when comparing the trajectory and other characteristics of jet flames of different fuels (e.g., propane and ethylene), the Froude number based on fuel characteristics, as defined in Eq. (2), has very limited value and can be misleading when interpreting results. In studies of far field flame characteristics, researchers such as Gore and Jian have opted to express results within the framework of the density under stoichiometric flame conditions [7]. Others such as Peters and Gottgens have utilized a modified form of the Froude number which combines initial jet and stoichiometric conditions [8].

Expressing Froude number in terms of the density of the constituents of the flame at stoichiometric conditions leads to Equation (3):

$$Fr^* = \frac{4Q}{\pi D^2 \left[gD \left| \frac{\rho_a - \rho_{j,flame}}{\rho_{j,flame}} \right| \right]^{1/2}} \tag{3}$$

The stoichoimetric conditions (flame temperature ~ 2400 K) corresponds to a density, ρ_{flame} of approximately 0.15 kg/m^3 for propane. As such, there is a multiplicative factor of 0.226 applied to Fr in determining the reference value, Fr*, for the propane flames and a factor of 0.061 for that associated with ethylene. Neither of these approaches to characterizing the influence of buoyancy is wholly satisfactory, especially for near-field conditions where the density can vary dramatically over the cross-section of the jet flame.

Integral methods have been used to discern the trajectory of horizontally-oriented issuing jets, and these approaches apply the momentum length scale, L_M. The effectiveness of this momentum length scale in collapsing the jet trajectory data for horizontally-issuiing buoyant, non-reacting jets is discussed in detail in the review article by Jirka [13] and by others [12, 14]. If one assumes all of the gas reacts under stoichiometric conditions, consistent with the definition of Fr*, the momentum length scale applicable to a horizontally-issuing flame, L_M may be determined by Equation (4):

$$L_M = \left(\frac{\pi}{4} \right)^{0.25} D * Fr^* \tag{4}$$

Given the finite time required for a reaction to take place, one might anticipate that the upward trajectory might be overestimated by this approach. Nonetheless, it provides a useful benchmark for this study.

2. EXPERIMENT OVERVIEW

This investigation attempted to illuminate the trajectory differences and species development for two fuels, propane and ethylene, issuing horizontally and combusting as a diffusion flame. These were studied over a range of Reynolds numbers and Froude numbers by changing the tube diameter and mass flow rate independently. For the purposes of this experiment fuels were stored externally to the AFIT Combustion Optimization and Analysis Laser (COAL) laboratory. The ethylene was stored in gaseous form, while the propane was stored in liquid form. The propane was vaporized using a Zimmer vaporizer, made by Algas. Both fuels were at or above 99.9% purity and are fed into the COAL lab through copper tubing and passing through an inline filter to remove any remaining impurities down to 0.5 microns. The fuel flow rate used in all experiments was controlled by a MKS, model 247D, four channel readout control panel and a corresponding MKS thermal mass flow controller. The flow controller provided the option of selecting fuel type for up to three different gases, and when fuel type was change the system was purged prior to data collection. After exiting the mass flow controller, the fuel traveled through a steel flex-line hose, which was attached to a bulkhead fitting and affixed to an angle bracket. Various exit tube diameters and fuel type were executed simply through connections on either side of the bulkhead. The fuel line was purged with nitrogen prior to connection to a different fuel type. Prior to the execution of any diagnostic technique, the fuel was spark ignited after the flow was initiated.

During testing, room ventilation was turned off and freestanding screens were used around the experimental station to accomplish several goals. First, the screens provided a safety barrier, limiting the propagation of high intensity UV light pulses. Second, the screens blocked most of any random air currents within the laboratory, to control the boundary conditions for the buoyant jet flows. Last, the screens also limited the possibility of incidental interference with the experimental set-up or hot combustion products. Room ventilation was turned back on following each test to remove combustion products.

Three different tube diameters were utilized during testing, with each tube being 16 inches (406 mm) long, and attached to an adapter which allowed it to mount directly to the bulkhead. The inside diameter for the three tubes were 7.75mm, 10.92mm, and 15.75 mm. All tubes were made to the same length with each having a tube length of at least 25 diameters to allow the flow to straighten and approach a fully developed laminar flow within the tube before the exit plane of the tube. All tubes were made to the same length. The bulkhead assembly, angle bracket, and fuel lines were all mounted on an Aerotech Automation 3200, three-axis traversing system. This allowed the laser sheet and camera to remain in a fixed position while the tube location was varied in the streamwise and vertical directions. The third axis of the traverse was fixed for this research. The experimental setup is portrayed in Figure 1.

To quantify the combustion process a Dantec Dynamics PLIF system was utilized for the experiment, as also shown in Figure 1. It was composed of a Quantel Brilliant B pulsed, frequency doubled neodymium-doped yttrium aluminum garnet (Nd:YAG) laser which provided a 532 nm beam to a Quantel tunable dye laser (TDL 90). The dye

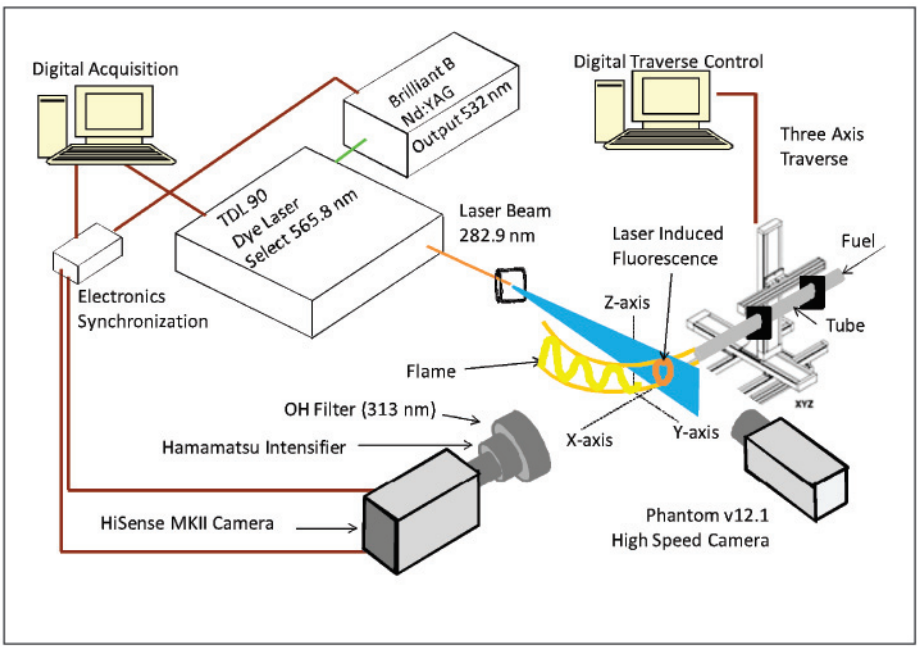

Figure 1. Experimental setup

was a combination of methanol and Rhodamine 590 in an aqueous solution. For these experiments the wavelength selected was 565.80590 nm. A frequency doubling crystal halved the wavelength to 282.90295 nm and was positioned in combination with a Pellin-Broca prism just prior to the beam exit. The precise position and rotational-orientation of the prism was computer-controlled to optimize output laser power. This wavelength was used to stimulate the hydroxyl radical and corresponded to the $Q_1(6)$ rotation vibration transition. The beam was spread into a laser sheet having a width of approximately 50 mm (2 inches) and thickness of 1 mm at the location where it intersected the flame.

The OH-PLIF detection system was composed of a camera, an intensifier, and a filter. The camera was a HiSense MkII camera with a progressive scan interline charged-coupled device with a pixel array of 1344 by 1024. A Hamamatsu Intensifier was required to amplify the light entering the camera. A band pass filter centered with a peak transmission of 59% at 313 nm and full-width-half-maximum of the peak transmission of 25 nm was positioned in front of the intensifier. A Quantum Composers, model 9514, delay pulse generator accepted the trigger employed to pulse the laser and in turn triggered the intensifier and the camera at the appropriate time to collect the fluorescence signal. The conditions for all tests conducted with propane and with ethylene are given in Table 1.

Table 1. Full test matrix for propane and ethylene.

Case Number	Fuel	Tube true ID, mm (and ref. OD)	Flow Rate (SLPM)	Reynolds Number	Cold Flow Froude Number, Fr	Reacting Flow Froude number, Fr*
1	Propane	7.75 (3/8 in)	0.49	300	1.06	0.24
2	Propane	10.9 (1/2 in)	0.69	300	0.63	0.14
3	Propane	15.7 (3/4 in)	0.99	300	0.36	0.08
4	Propane	7.75 (3/8 in)	1.62	1000	3.49	0.79
5	Propane	10.9 (1/2 in)	2.29	1000	2.09	0.47
6	Propane	15.7 (3/4 in)	3.30	1000	1.19	0.27
7	Propane	7.75 (3/8 in)	2.44	1500	5.26	1.19
8	Propane	10.9 (1/2 in)	3.43	1500	3.13	0.71
9	Propane	15.7 (3/4 in)	4.95	1500	1.78	0.40
10	Propane	7.75 (3/8 in)	0.23	142	0.5	0.11
11	Propane	10.9 (1/2 in)	0.55	240	0.5	0.11
12	Propane	15.7 (3/4 in)	1.37	412	0.5	0.11
13	Propane	7.75 (3/8 in)	0.46	283	1.0	0.23
14	Propane	10.9 (1/2 in)	1.09	476	1.0	0.23
15	Propane	15.7 (3/4 in)	2.79	840	1.0	0.23
16	Propane	7.75 (3/8 in)	0.69	425	1.5	0.34
17	Propane	10.9 (1/2 in)	1.64	716	1.5	0.34
18	Propane	15.7 (3/4 in)	4.10	1234	1.5	0.34
19	Ethylene	7.75 (3/8 in)	0.98	300	7.67	0.47
20	Ethylene	10.9 (1/2 in)	1.38	300	4.57	0.28
21	Ethylene	15.7 (3/4 in)	2.01	300	2.63	0.16
22	Ethylene	7.75 (3/8 in)	3.27	1000	25.58	1.57
23	Ethylene	10.9 (1/2 in)	4.62	1000	15.31	0.94
24	Ethylene	15.7 (3/4 in)	6.70	1000	8.75	0.55
25	Ethylene	7.75 (3/8 in)	4.91	1500	38.41	2.36
26	Ethylene	10.9 (1/2 in)	6.93	1500	22.97	1.41
27	Ethylene	15.7 (3/4 in)	10.05	1500	13.13	0.82

In order to complement the PLIF data, two types of high speed images were captured for a subset of the experiments using a Vision Research Phantom v12.1 camera. The first type were unfiltered visible light images, while the second was filtered to 432 nm +/- 5 nm, to capture the CH* radical chemiluminesence as an additional marker for combustion regions. For both types of imaging the camera was placed perpendicular to the plane defined by the jet trajectory, approximately 1.2 meters away. The Phantom camera was used in conjunction with a Micro-Nikkor 105mm f/2.8 lens and operated at 6200 frames per second, for the unfiltered images, and about 100 frames per second for the filtered images with exposure time maximized for both sets of images. The increased exposure time was required to collect enough light through a very narrow bandpass filter. These images provided a side view over an extended range of the reaction zone volume while PLIF data was based on planar cross-sections of the reaction zone which were normal to the streamwise direction. The unfiltered images tended to be dominated by red/orange regions, probably blackbody emission from hot

soot. This blackbody emission is eliminated in the filtered data. While approximately 0.8% of the radiated power of 2000 K soot could be in the visible range, only about 0.014% of the energy was below 440 nm, and about 0.0015%, or about 0.2% of the visible energy, would pass through the band pass filter used on the camera, and this percentage would be even lower if the soot temperature is lower [15]. Thus, the molecular emission of CH* at 432.5 nm should dominate the 430-440 nm filter.

In implementing PLIF, this research entailed analytical consideration of the conditions under which OH^- is preferentially formed. Using the NASA Chemical Equilibrium with Applications (CEA) code, the equilibrium products of combustion for both propane/air and ethylene/air combustion at one atmosphere were computed across a broad range of equivalence ratios, from very lean to very rich. As expected, the production of OH^- should be highest at equivalence ratios near 0.8, slightly lean, but near stoichiometric, and is nearly extinguished by an equivalence ratio of 1.4 for both fuels. It can, therefore, be safely assumed that the regions of highest OH^- concentration should correspond to the near-stoichiometric combustion regions, and that when the OH^- concentration is nearly zero (no signal), then the mixture must be either too rich or too lean for combustion. It is conceivable that the OH^- might be produced elsewhere and transported to the interrogation plane. However, the hydroxyl radical has a very short lifetime, and the velocity is relatively low, and so the regions of fluorescence, by and large, correspond to OH^- production regions. Given the combustion limits of propane and ethylene at one atmosphere (propane: $0.52 \leq \varphi \leq 2.4$, or 0.021 to 0.095 volume fraction; ethylene: 0.027 to 0.36 volume fraction), the OH^- generation zone is expected to be near the outside of our diffusion driven flames, with a much greater chance of merged OH^- and PAH regions in the ethylene [16].

There are many valuable sources in the literature which document the behavior of combustion using Planar Laser Induced Fluorescence (PLIF) of the hydroxyl radical (OH^-) or other species, such as polycyclic aromatic hydrocarbons (PAH). A factor for PLIF measurements is that PAH, which form during the reaction, also fluoresce and provide a signal, as documented by a number of authors [17, 18, 19]. Fortunately, the nature of the fluorescence is broadband, and so by tuning the laser it is relatively straightforward to distinguish the signal from the OH^- from the PAH. In principal, having two separate entities providing a signal could be somewhat problematic due to the ambiguity of the data. However, in many situations, the regions of the two species do not overlap spatially as experienced in the current data. The PAH signal is predominant in the fuel rich regions of the flame. Therefore, the OH^- signal, which is prevalent in stoichiometric to fuel-lean regions can be isolated from the PAH signal. Previous researchers have used this to their advantage in separating the fluorescence within a given image. One example of this applied to OH^- and PAH formation is given by Böhm et al. where the authors took advantage of the spatial segregation of the two species in analyzing their data [20]. Williams et al. provide a second example of the use of spatial segregation to take data for the two species simultaneously, which is described in more detail below [21].

It is noteworthy that the reaction pathways whereby PAH forms are, in and of themselves, a subject of ongoing research in the larger community. This is in part due

to the fact that some PAH isomers, such as benzo-z-pyrene, are potentially toxic. Yamamoto et al. used a counterflow burner system and measured species concentration. They found that strain rate has a strong influence on high-molecular-weight combustion intermediates and suggest that development of detailed kinetic mechanisms describing formation and destruction of intermediates such as PAH are still needed [22]. While the effect of buoyancy— rather than chemical kinetics— is the main focus of the current investigation, the measurements of regions of high PAH concentrations may also guide the development of such models. It is noteworthy that the region of PAH formation in the current research should be essentially oxygen free, as the oxygen entrained in the shear layers around the jet should be consumed in the outside combustion region, characterized by the formation of OH^*. This implies that the PAH formation pathways present in this research should not involve oxygen, but could involve nitrogen or trace components of air, either as participating species or catalysts.

3. RESULTS

Initially, the flame was investigated using the unfiltered Phantom camera. A typical set of images collected for one example (Case 7 of Table 1) are shown in Figure 2, which provides some insight into the nature of the presentation to come. Here and in

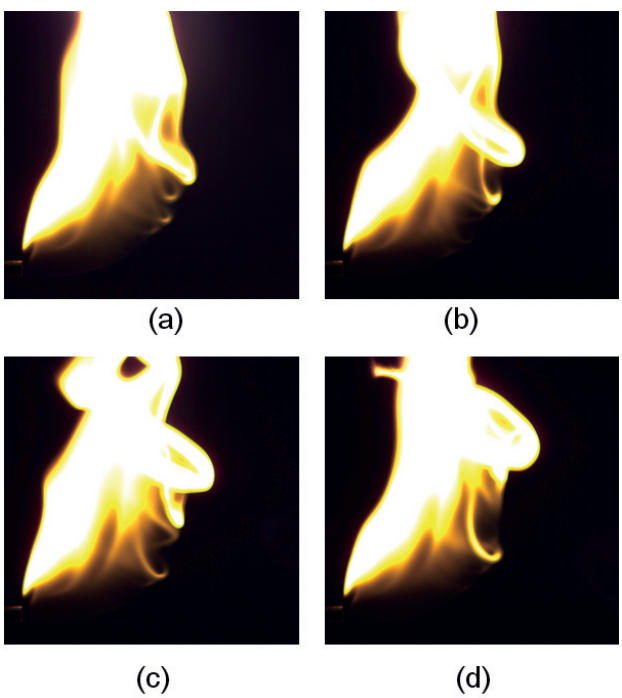

Figure 2. Instantaneous flame pictures of case 7 (Re = 1500, Fr* = 1.19) at reference times of (a) t = 0, (b) t = 0.0322 sec, (c) t= 0.0645 sec, and (d) t = 0.0967 sec.

subsequent images, the images are shown so that the streamwise direction is presented as left-to-right, and the tube is visible in the lower left portion of each image. The images were collected with a side view of the flame at the high frame rate, and an exposure time of 0.00016 seconds. The bright region immediately downstream of and above the exit indicates the generally upward trajectory of the flame for one representative experiment. This region would be expected to contain the highest temperature products of combustion from fuel initially toward the bottom of the jet, as well as some ongoing combustion processes of fuel initially at the top of the jet. The lower portion of the flame is dimmer but also indicates an upward trajectory, albeit less steep than the upper region of the flame. The lower extremity of the flame is visible due to the somewhat longer integrated path through the combustion region possible at the bottom of the flame. The region in the middle, to each side of the centerline of the jet core, is quite dim. This is a product of 1) the buoyancy driven flow keeping the combustion region quite thin on the sides, leading to short pathlengths through the medium, and a lower emission in the direction of the camera, and 2) the sweeping of the hot products upward. In some cases, like the one shown here where the Reynolds number was moderately high, the growth of vortices along the lower edge of the flame could be identified and tracked in time. In general, it was more difficult to identify specific features along the mixing region on the top side of the flame. Each collection of 2,000 instantaneous images was averaged to gain an understanding of the overall features of the flame.

As documented in Figure 3, this procedure was executed at one location downstream of the tube exit for a sample case, and it was clearly seen that the signal due to OH^- was present only for a very discrete range of wavelengths near 282.909 nm while the PAH signal was present when stimulated through a much broader range of wavelengths. Having two separate entities providing a signal can, in general, be problematic due to the ambiguity of the data. However, it is an issue which has been addressed in the literature by Williams et al. who performed a study of vertically-oriented buoyant diffusion flames subjected to acoustic forcing [21]. The authors focused on the region within approximately 5 diameters of the tube exit and presented results, emphasizing

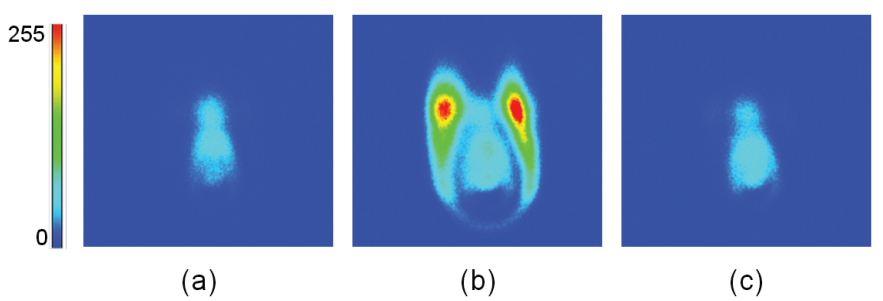

Figure 3. Example of PLIF images (Case 4 at X/D = 3) for varied laser wavelength with given measured intensity in the accompanying colorbar: (a) 282.897 nm, (b) 282.909 nm, and (c) 282.917 nm.

that the region containing the hydroxyl radical was present in the fuel-lean region while the PAH was present in the fuel rich region. Due to the spatial segregation of the two species in that instance, it was actually an advantage for both species to be detected. In another study, Won et al. utilized a counterflow burner which yielded a 2 mm separation between detected lines of PAH and OH^- when interrogated by a laser of the appropriate wavelength. This spatial separation of the two species permitted an analysis of chemical heat release rate through the reaction of OH^- with other entities, specifically as it relates to toluene blending [19].

In the current study, the relative locations of the OH^- and PAH were consistent with expectations and the literature in that the OH^- tends to form in fuel-lean regions while PAH tends to form in fuel-rich regions, and the example represented in Figure 3 bears this out. Very near the tube exit ($X/D < 0.5$), it was generally the case that only a single, nearly axisymetric region of OH^- production of approximately the diameter of the tube was detected. In some instance, depending on Reynolds number and Froude number, the overlap of the two species did not occur until X/D exceeded 8, though under other flow conditions the overlap occurred considerably closer to the tube exit. The majority of results herein correspond to situations where the OH^- and PAH are, apparently, spatially segregated. It is also worth noting that, inferring from [19], if these regions do indeed overlap, the PAH compounds are also being consumed as they are being formed, due to the presence of oxygen and enough thermal energy to overcome any reaction initiation barriers.

The rapid upward ascent of the flame shown in Figure 2 suggests the primary reason the laser was introduced horizontally rather than vertically. It would have been difficult to collect well-resolved PLIF signal throughout the entire vertical slice of the flame due to it large dimension for many flames studied. This configuration would also have led to other inconveniences, related to safety, when implementing the experiment, and so all images were acquired with the laser sheet propagating horizontally. In some cases, this configuration choice led to the exclusion of PLIF data for the upper regions of the flame, so our focus was placed on the many interesting features which were resolvable in this experiment.

3.1 Flame Development

One of the goals was to gain some level of understanding of the relative effects of Reynolds number and Froude number on flame development and trajectory. To this end, one of the more insightful results is given in Figure 4 where time-average propane flame visualizations are shown for Cases 7, 8, and 9. Each image has been resized so that the normalized distances are identical. The left column shows unfiltered images of the flame, where the signal is dominated by soot formation. The right column presents filtered images where the primary contributor to the signal are combustion intermediates (CH^*). Note that in the experiments, the tube diameter changed while the camera position was held fixed. Therefore, to represent the data as normalized by jet diameter, the images were resized to show the tube diameter using the same resolution. The resized filtered image for the $Fr^*=0.40$ case led to a smaller image size since the tube diameter was large, and a gray matte is shown for this (lower right) image.

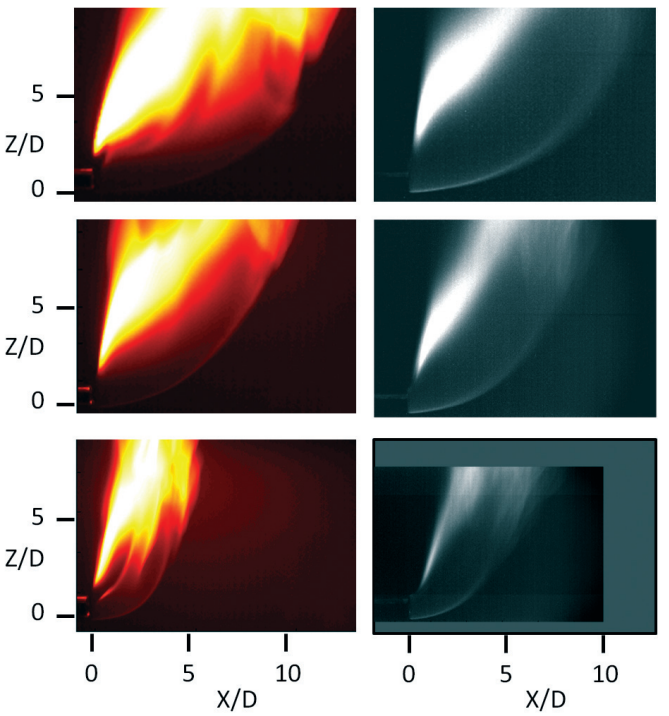

Figure 4. Time-averaged flame visualizations for Re = 1500 and varied Froude number (top: Fr* =1.19, center: Fr* = 0.71, bottom: Fr* = 0.40)

The Z/D = 0 location here corresponds to the lower edge of the jet to maintain consistency with OH-PLIF data rather than the centerline, which is sometimes used as the convention. The brightest portion of each image appears along the upper contour of the flame. Meanwhile the lower portion of the reaction zone, while dimmer, is well-defined and easily identifiable in each image. With a fixed Reynolds number (Re = 1500), the strong influence of reacting Froude number on the flame development and trajectory is clear. The top image of Figure 4 corresponds to the averaged image of the temporal progression shown in Figure 2. As reacting Froude number decreases from 1.19 to 0.40, the flame trajectory clearly steepens, suggesting that the reacting Froude number has a significant impact on the flame development.

For these conditions, PLIF proved to yield tremendous insight into the details of reaction zone. In Figure 5 , the PLIF data is shown for the Re=1500, Fr* = 1.19 case (Case 7) corresponding to the top image in Figure 4. In this representation, averaged images from the camera are presented. The development of the OH^- is already quite pronounced by 0.78 diameters downstream. The reaction zone defined by OH^- at this location takes the outline of a teardrop shape, and clearly the concentration of OH^- is much higher in the upper portion of the shear layer. It is noteworthy that the OH^- region defines both the outer extent of the flame, and is much more pronounced on the upper

side of the flame. Within the region encompassed by the OH^- fluorescence and nearer to the core, a region of PAH may be seen, albeit with lower intensity. The PAH apparently marks the boundary between the core fluid and the reaction zone in the fuel-rich region. At the X/D =1.56 location, the outer region indicating OH^- appears U-shaped and does not encompass the entirety of the jet. Without knowledge of the overall flame behavior, one might interpret the OH^- data from downstream locations to indicate a lack of OH^- formation on the upper side of the flame. Rather, the images from X/D = 1.56 downstream simply do not show the topmost portion of the flame due to limitations in the laser sheet width combined with the rapid ascent of the upper portion of the flame as indicated in Figure 4. While some consideration was given to reorienting the laser sheet to propagate vertically through the flame, but it was reasoned that, especially for some low Fr* cases, the vertical extent of OH^- propagation would lead to poor measurement resolution due to the spatial resolution of the camera, increased absorption of OH^- along the pathlength of the laser sheet, and increased soot opacity between the camera viewing position and the flame. As such, the topmost extent of the occurrence of OH^- at locations downstream of X/D = 1 can only be said to be indeterminate from the data presented here.

The PAH formation and production can be seen throughout all planes represented in Figure 5. Its initial formation can be seen by X/D = 0.78, and concentration tends to increase with X/D as combustion takes place. The PAH forms well inside the layer of OH^- and clearly deviates from axisymmetry, which can be seen most clearly for the X/D = 1.56 to 3.12 planes. The most obvious attribute of the PAH concentration profile is the indentation on its upper extent. It would appear that the PAH plunges downward

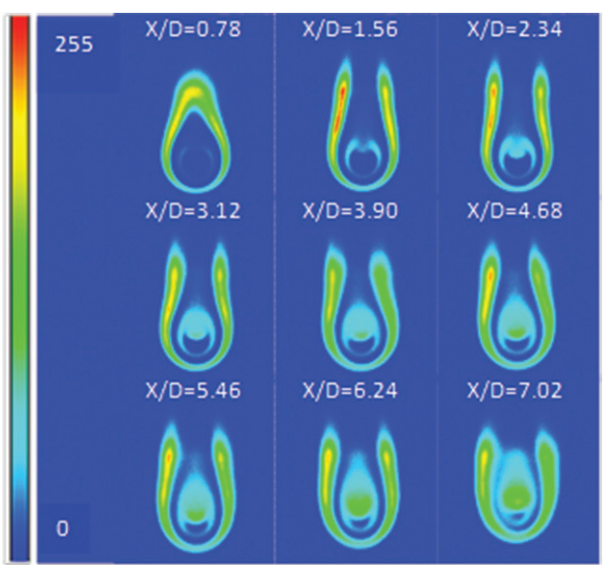

Figure 5. PLIF visualizations for Re = 1500, propane, Fr* = 1.19.

into the core as the jet propagates downstream. This downward motion is likely driven by buoyant effects. The combustion region, and the outer layers of the jet are being heated, and the density is dropping, resulting in upward motion due to buoyancy. This upward motion causes an upward shear on the outer layers of the fuel core flow, and the visualizations suggest that two counter-rotating vortices are formed within the core. Near the top center of the core jet, the PLIF visualizations indicate that the flow must be somewhat downward, relative to the left or right outside edges. This depiction of the flow pattern is consistent with the velocimetry results, concentration data, and flow visualizations given in the literature for horizontally issuing buoyant jets, with the shape of the jet sometimes described as a 'veil' [23, 24].

The larger PAH signal in the top of the core of the jet also is attributed to the heating of the core fuel driving the reactions that form the PAH from the propane or ethylene. Since the higher temperature parts of the oxidation region in the diffusion flame are at the upper side, more PAH than the lower region. By X/D = 7.02, the enclosed region of what one would expect to be core fluid (fuel) appears only near the low edge of the jet while the regions of OH^- and PAH have nearly merged by this location.

A more quantitative spatial representation of the flame propagation based on OH-PLIF for the same case is provided in Figure 6. Here and in other figures to follow, note that the X-axis is elongated compared to the Y- and Z- axes in order to permit a perspective view of the PLIF cross-sections, and so the upward trajectory of the flame is actually larger than it might appear at first glance, as indicated by the scale of the Z-axis. In this representation, the planar images of Figure 5 are combined with the traverse position to yield the spatial location of the PLIF data, leading to a representation of the flame trajectory.

The PLIF data was also gathered in a similar fashion for the Fr* = 0.71 and Fr* = 0.40 cases represented in Figure 4. These results are presented in Figure 7 for Fr* = 0.71

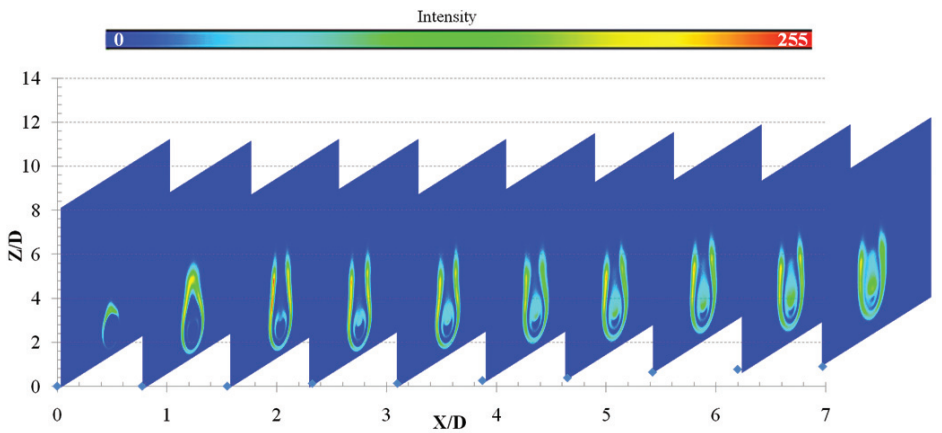

Figure 6. Streamwise progression of averaged PLIF images for propane (Re = 1500, Fr* = 1.19). X/D = 0.1, 0.8, 1.6, 2.3, 3.1, 3.9, 4.6, 5.4, 6.2, and 7.0.

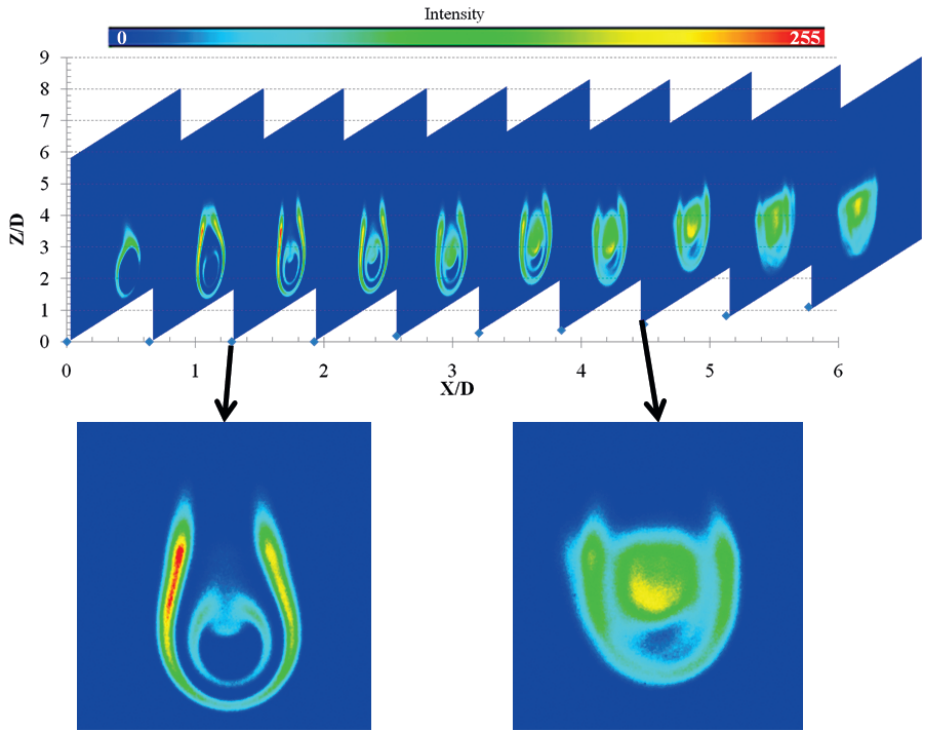

Figure 7. Streamwise progression of averaged PLIF images for Re = 1500, Fr* = 0.71. X/D = 0.1, 0.6, 1.3, 1.9, 2.6, 3.2, 3.8, 4.5, 5.1, and 5.8 with insets at X/D = 1.3 and 4.5.

and in Figure 8 for Fr* = 0.40. For sake of brevity, the spatial representation is combined with insets of two full planar views for each case. An interesting finding is that the evolution of both the OH^- and PAH take on similar characteristics for these three cases, despite the substantial difference in Froude number and the upward flame trajectory seen in the visualization of Figure 4. For example, the PAH formation initiates within the bounds of the OH^-, and includes the same pattern of indentation on the upper portion of the flame. Despite these similarities, there are noteworthy differences between the three cases. For example, the increased gradient of the trajectory, combined with the larger tube diameter and fixed laser sheet height does result in an incomplete picture of the OH^- profile by X/D = 0.3 for the Fr* = 0.40 case. Furthermore, investigating a consistent location on the X-axis, it can be seen that the upward trajectory increases as Froude number decreases, consistent with the flame visualization.

To gain a broader understanding of the influence of Reynolds number on the development of the combustion zone, additional measurement sets were collected for a fixed Reynolds numbers of 1000 and 300, each with varied Froude number. The three

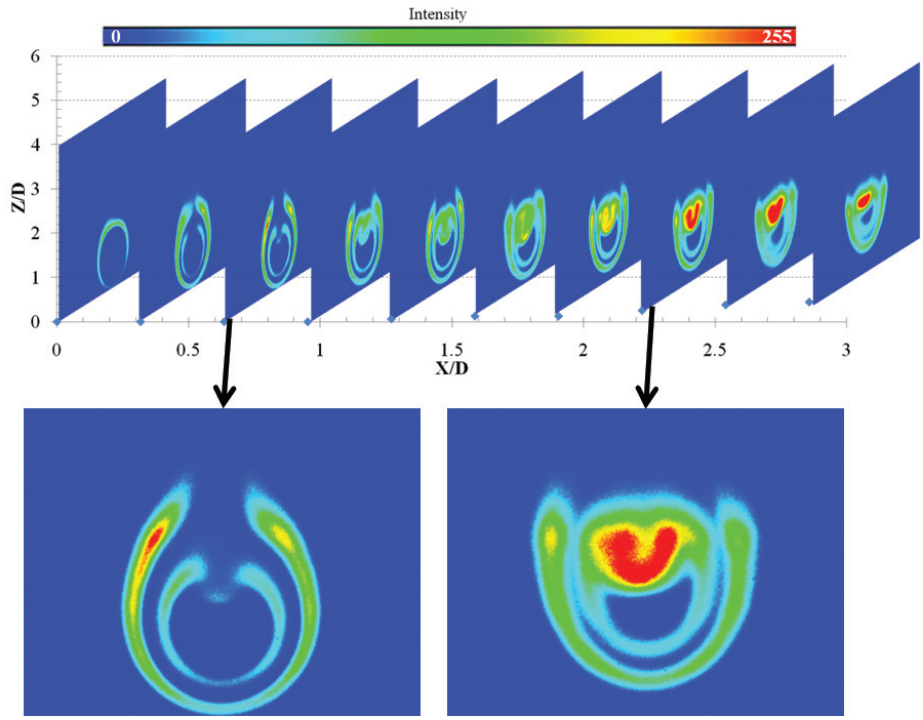

Figure 8. Streamwise progression of averaged PLIF images for Case 9, propane, Re = 1500, Fr* =0.40. X/D = 0.1, 0.3, 0.6, 0.9, 1.3, 1.6, 1.9, 2.2, 2.5, and 2.9 with insets at X/D = 0.6 and 2.2.

sets of PLIF data for Re=1000, corresponding to conditions listed for Cases 4-6 in Table 1, are provided in Figure 9 while the three sets of PLIF data for the Re=300 case (Cases 1-3) are given in Figure 10.

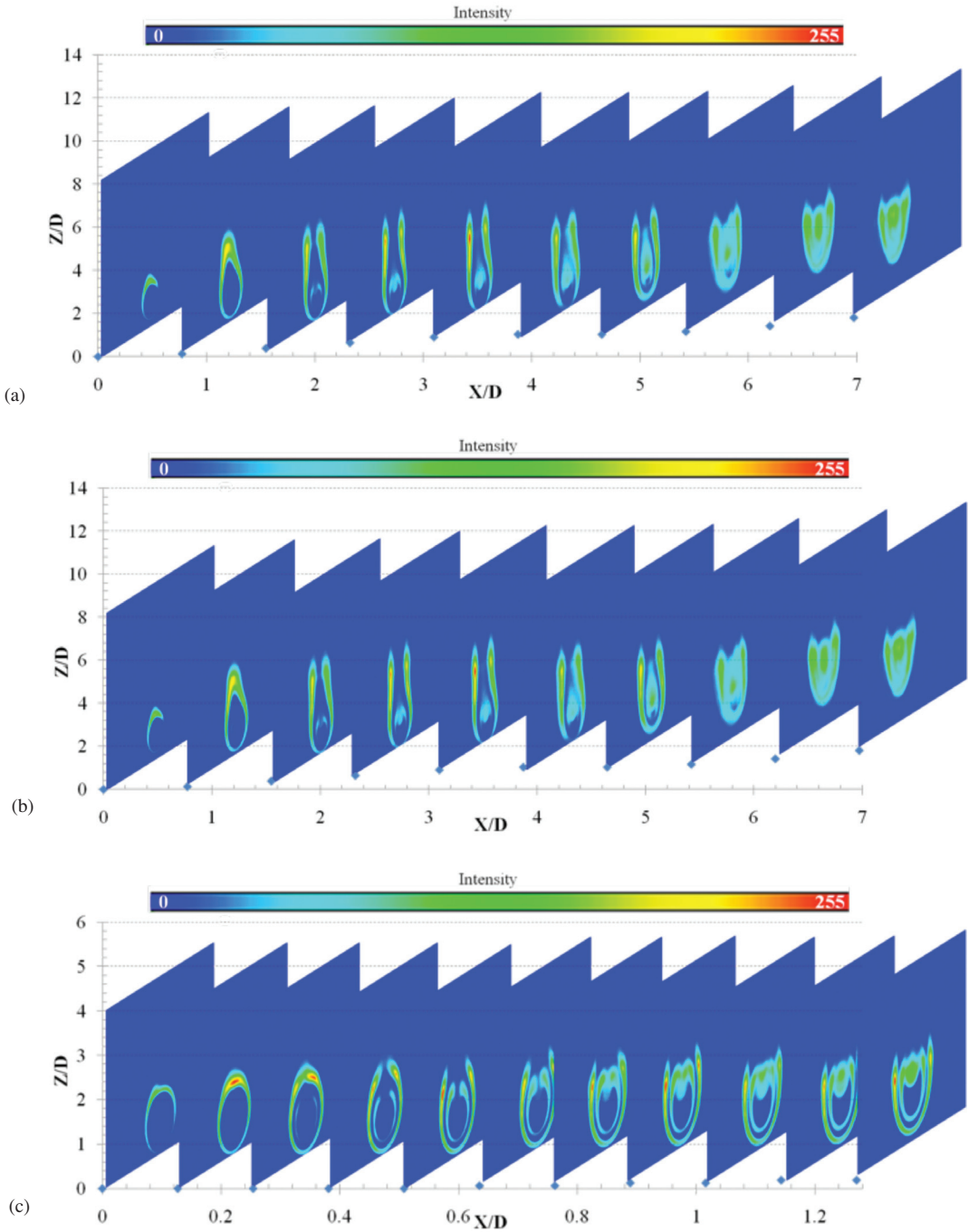

Figure 9. Re = 1000, (a) Fr* = 0.79, (b) Fr* = 0.47, (c) Fr* = 0.27.

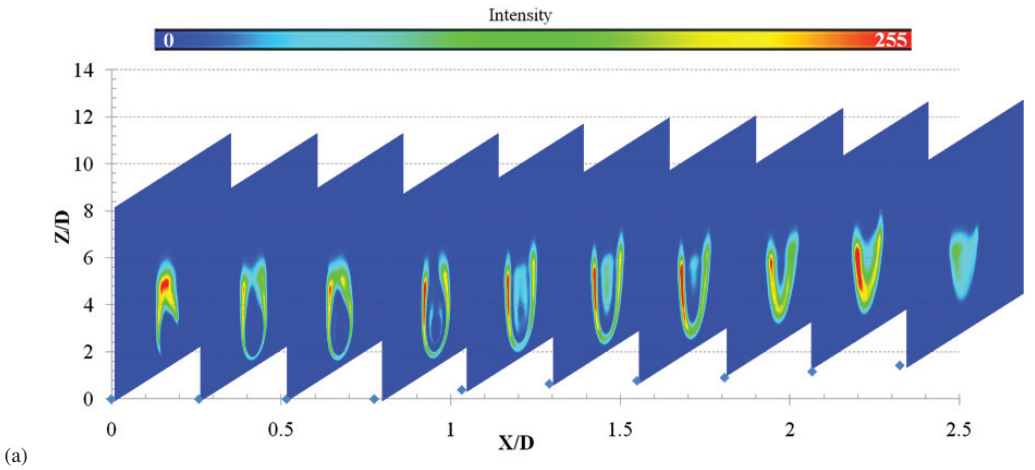

(a)

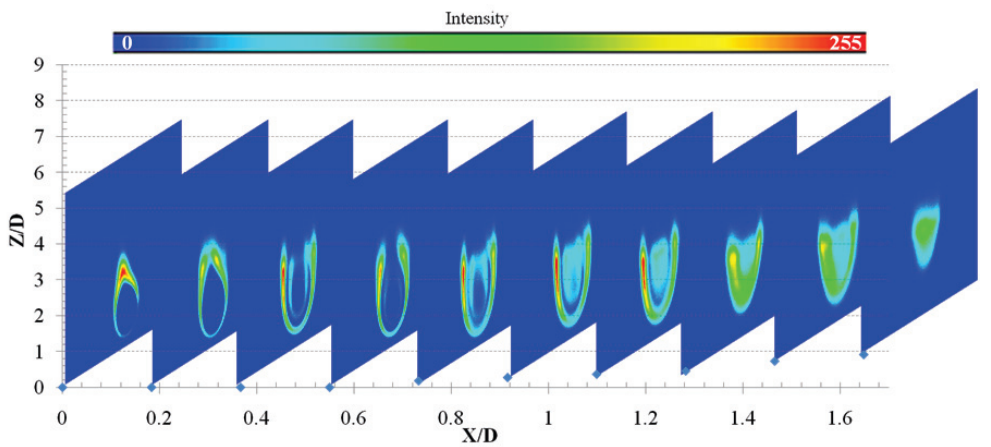

(b)

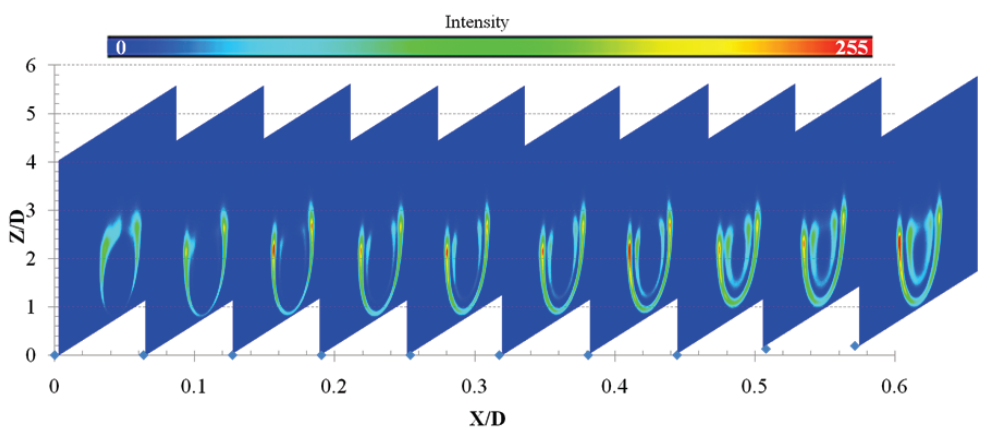

(c)

Figure 10. Re = 300, (a) Fr* = 0.24, (b) Fr* = 0.14, (c) Fr* = 0.08.

As Froude number decreases, the upward trajectory of the flame becomes more prevalent, as indicated by the smaller values for X/D on these figures. However, taking that attribute into account, one of the more revealing aspects of Figure 9 and Figure 10 is that reducing the Reynolds number to 1000 and then to 300 had little effect on the overall trends for the OH^- and PAH compared to the Re=1500 case.

Since any slight changes might be obscured by the dramatic changes in flame trajectory, additional tests were carried out for cases where the Froude number was held fixed and the Reynolds number varied. The rationale for these additional data sets was that flame trajectory was expected to trend primarily with Froude number. Time-averaged flame visualizations, shown in Figure 11 showed that the low Reynolds number flame (Re = 426) did not propagate quite as far downstream as the two higher Reynolds number cases. Once more, the right column shows unfiltered images of the flame, whereas the right column presents filtered images of, primarily, CH^*. However, the differences in trajectory were far less pronounced than those given in Figure 4, where Froude number, rather than Reynolds number, was varied.

Corresponding PLIF data for the fixed Froude number (Cases 16-18 from Table 1) are given in Figure 12. The data confirmed that the qualitative features of the development for OH^- and PAH was for the most part independent of Reynolds number.

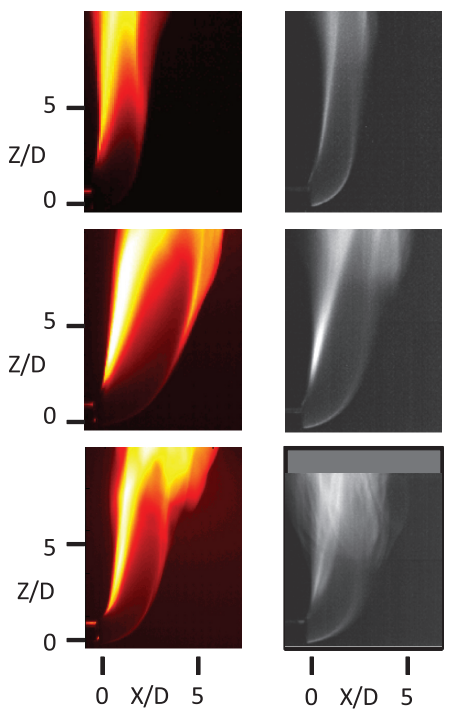

Figure 11. Time averaged flame visualization for Fr* = 0.34 and Re= 426 (top), Re = 716 (center), and Re = 1230 (bottom) for unfiltered (left column) and filtered to show CH* (right column).

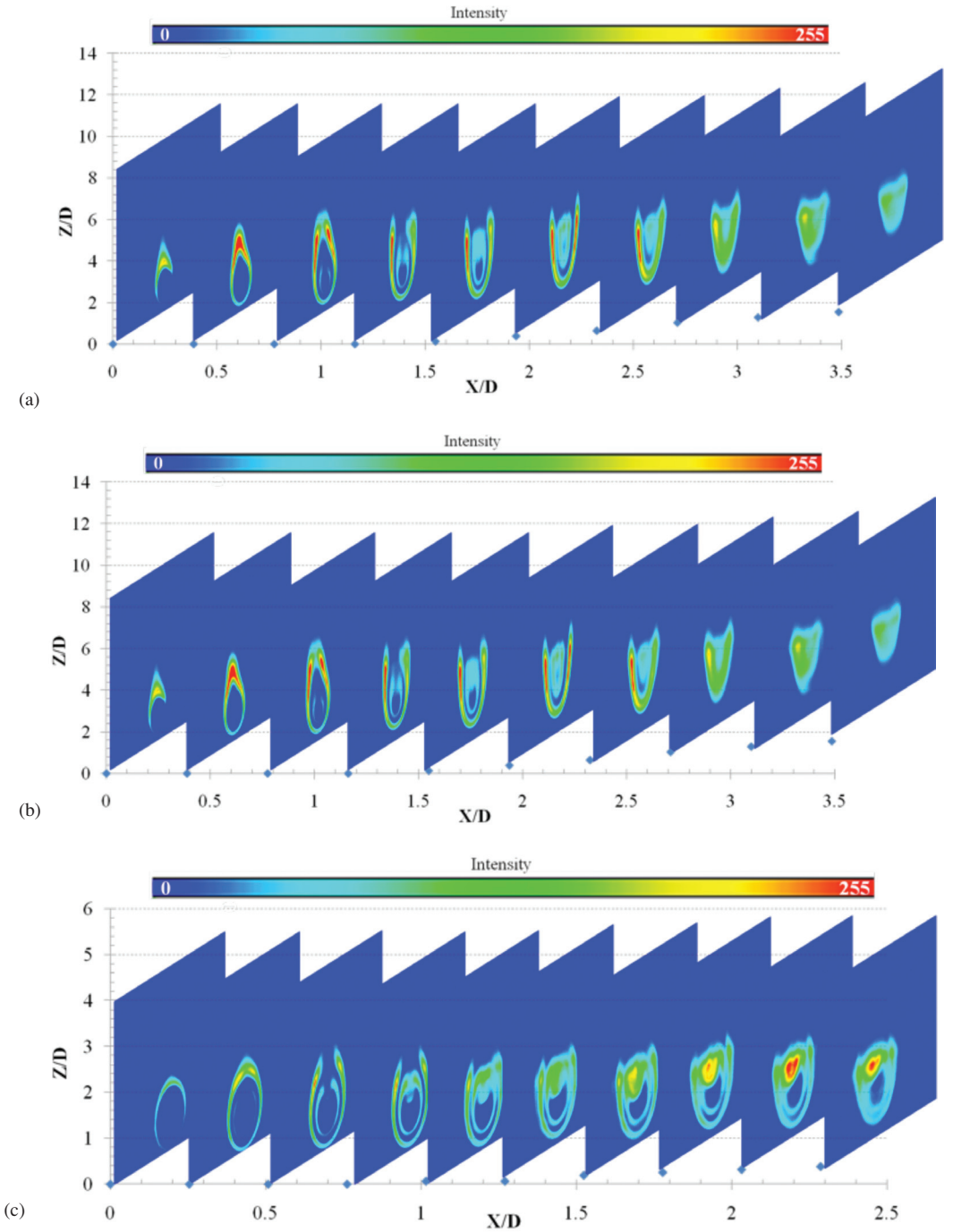

Figure 12. Averaged PLIF data for Fr* = 0.34 and (a) Re =426 , (b) Re =716 (c) Re =1230.

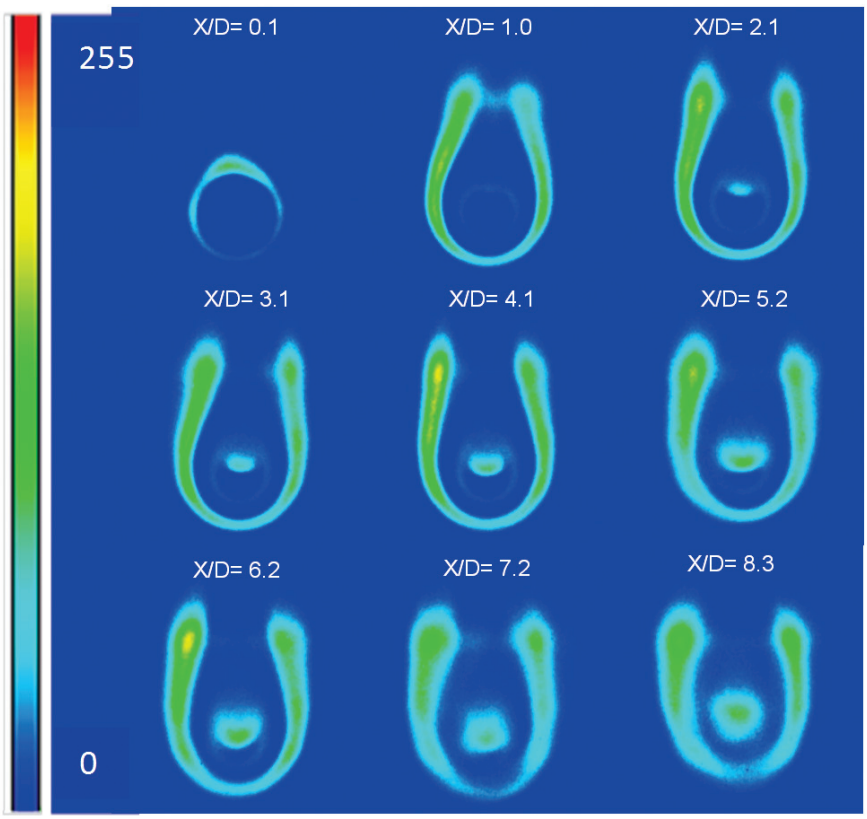

Figure 13. PLIF visualizations for Re = 1500, ethylene, Fr* = 2.36 for the indicated X/D.

One question raised by the pattern of development of the region of high PAH concentration was whether fuel type would influence trends and behavior. This was addressed by performing test cases with ethylene in place of propane. In Figure 13, the PLIF images are shown for Case 25, which is ethylene operated with similar jet Reynolds number conditions for the propane test given in Figure 6 (for propane). Initially, OH^- formation is nearly axisymmetric, but by one diameter downstream the signal indicates a rapid vertical ascent of the upper portion of the flame reaction zone. In the same X/D =1.0 image, the PAH formation can be seen in a faint nearly-axisymmetric outline. By X/D = 2.1, it is obvious that the region of PAH grows much more rapidly on the upper portion of the jet flame. Furthermore, the same pattern of formation, appearing as a downward indentation of the jet core, is as evident for ethylene as it was for propane. This general qualitative similarity for the two types of fuel was seen throughout testing as long as the Reynolds and reacting Froude numbers were close to one another.

Spatial representation of this data set and two other data sets corresponding to ethylene fuel with the Reynolds number set at 1500, as reacting Froude number is

varied, are given in Figure 14. Clearly, the nature of the evolution of OH^- and PAH was largely unchanged, even when the fuel was switched from propane to ethylene.

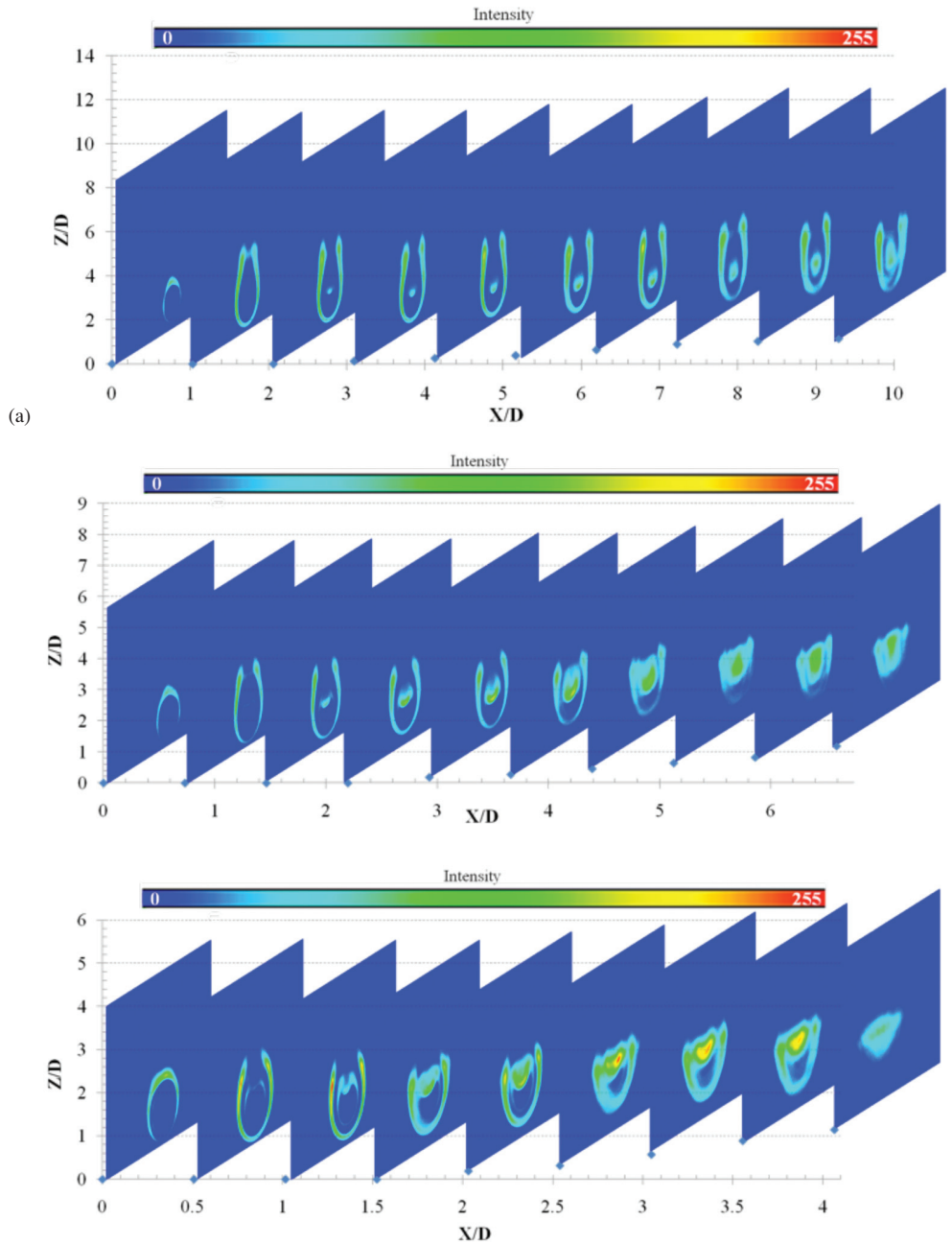

Figure 14. Averaged PLIF data for ethylene with Re=1500 and (a) Fr*=2.36, (b) Fr*=1.41, (c) Fr*=0.82.

Additional details of PLIF measurements carried out for ethylene and propane in Table 1, is given by Ref. [25].

3.2 Flame Trajectory

While one might argue that the most compelling aspect of the PLIF data is the persistent qualitative aspects of the combustion zone, a second output is the flame trajectory itself. The well-defined lower edge of the flame from the PLIF data was selected as the basis for the trajectory (based on an intensity threshold) and the origin [(X, Z) = (0, 0)] corresponds to the bottom of the tube exit. The trajectory data for Re=300, 1000, and 1500 are given in Figure 15, where, the influence of the reacting Froude number is clearly elucidated. For the Re=300 data shown in Figure 15(a), the turning of the flame is strong such that only a limited streamwise set of data were collected for each case. The lowest Froude number case (Fr* = 0.08) shows that the lower edge of the flame has shifted upward by 0.24D by station X = 0.57D. For the highest Froude number case of this plot (Fr* =0.24), the same Z/D position is attained by approximately X/D = 1. For Figure 15(b) and (c), the initial trend of the defined trajectory, indicated by the presence of the hydroxyl radical, is slightly downward due to the negative buoyancy of propane gas relative to air. However, for each data set, the trend reverses to an upward trajectory shortly downstream of the tube exit as the density decreases. A definitive trend of upward trajectory as the reacting Froude number decreases is clearly prevalent for each Reynolds number.

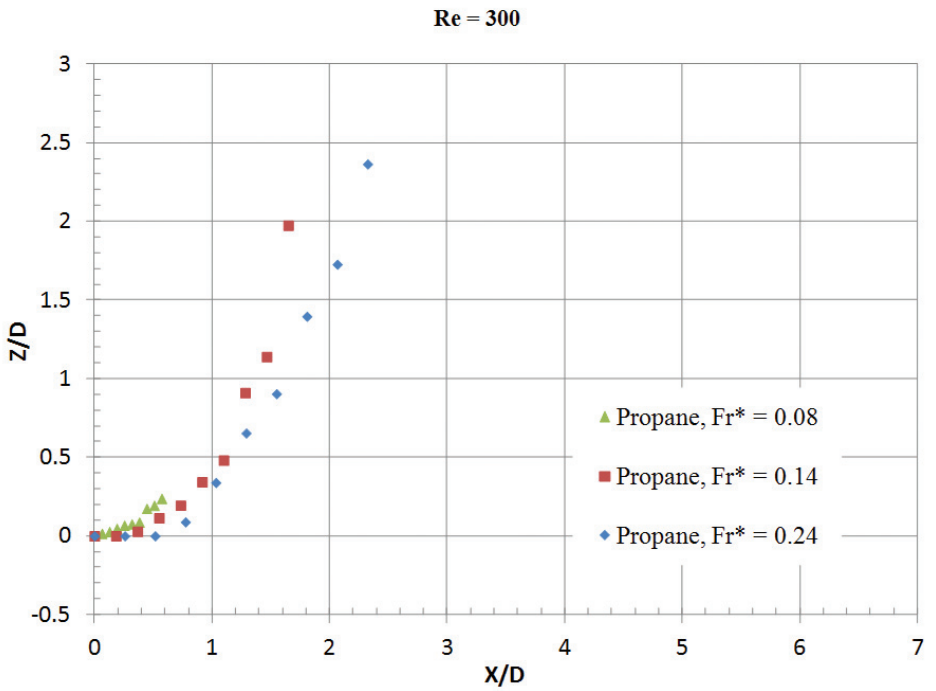

(a)

Figure 15.(to continue)

(b)

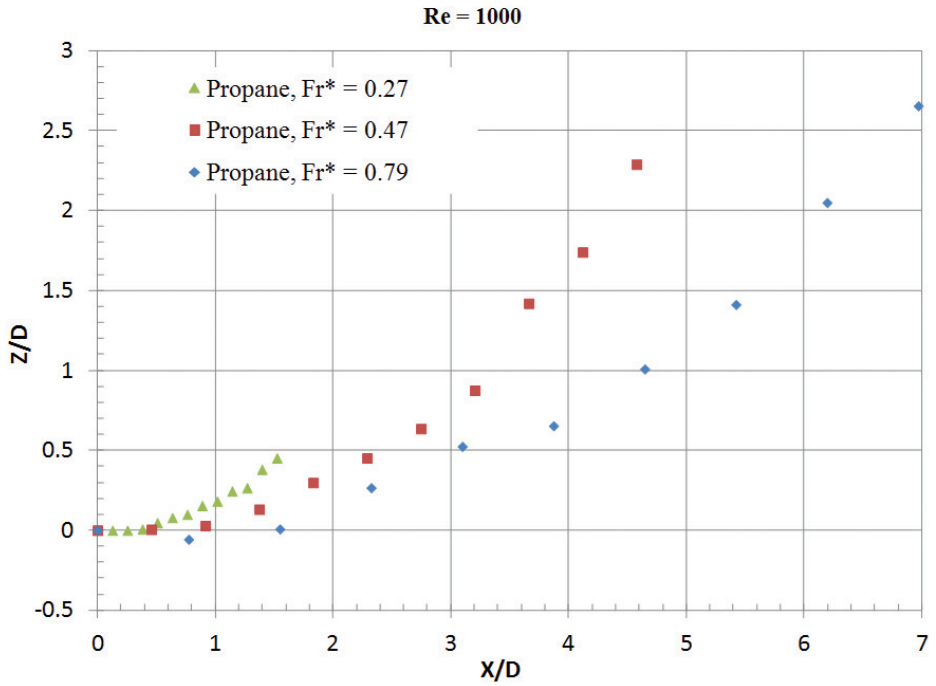

(c)

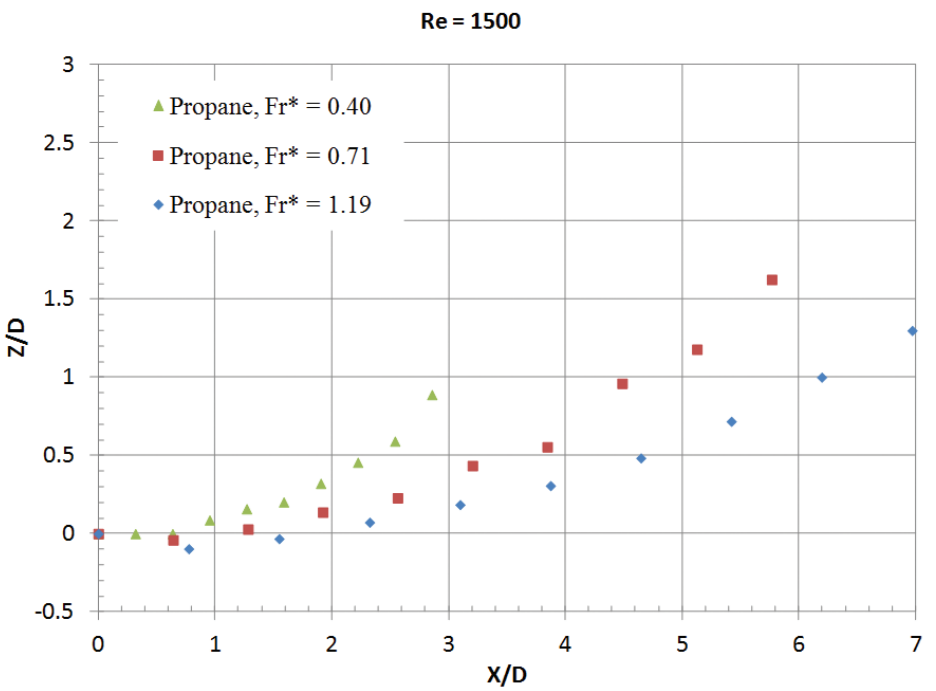

Figure 15. Trajectory data for variable reacting Froude number and fixed Reynolds number (a) Re = 300, (b) Re = 1000, and (c) Re = 1500.

To clarify the level to which the trajectory is affected by Reynolds number, trajectories were also computed for cases with Froude number held fixed while Reynolds number varied. These results are given in Figure 16. Contrasting the respective plots for Fr* = 0.23 in Figure 16(a) and Fr*= 0.34 in Figure 16(b), each with the same scaling, the effect of Froude number is evident. The changes in the trajectory

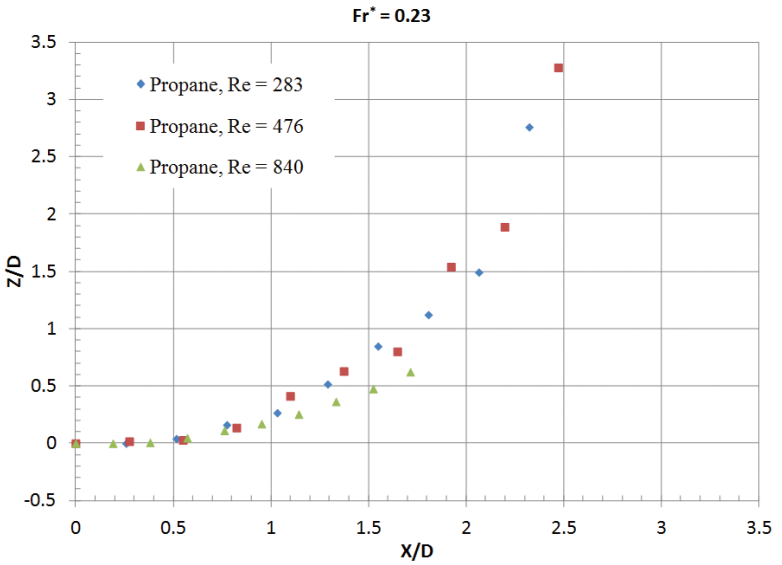

(a)

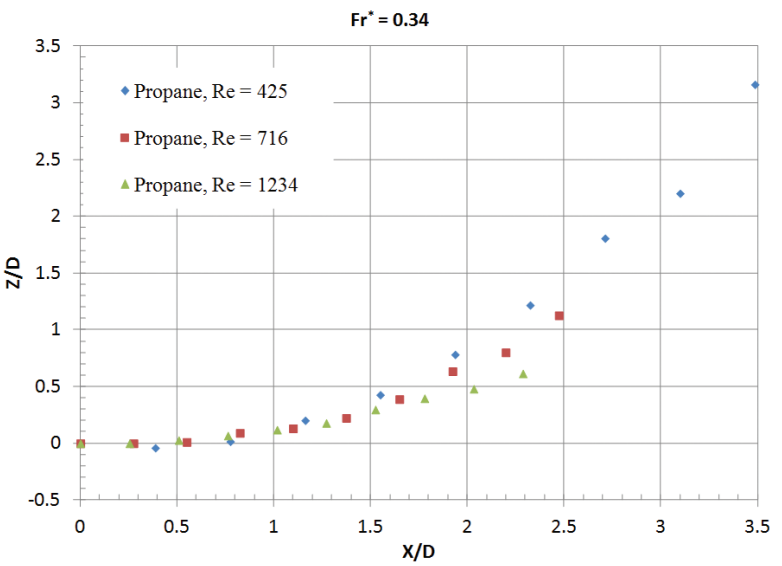

(b)

Figure 16. Trajectory for varied Reynolds number and fixed Reacting Froude number (a) Fr* = 0.23 and (b) Fr* = 0.34.

plots as the Reynolds numbers increases are much smaller, though for both cases there is a tendency for the trajectory to flatten with increasing Reynolds number. This delay in upward motion may be attributable to the relative differences between the ratio of reaction time to fluidic time.

The trajectory data may also be considered with reference to the momentum length scale, L_M, defined in Equation (4) using Fr^*, and the outcome is given in Figure 17. While there is some scatter from case to case, the data does appear to collapse to a reasonable first approximation for the two fuel types. The plots clarify the delay in upward trajectory, presumably due to the time required for the diffusion flame to react

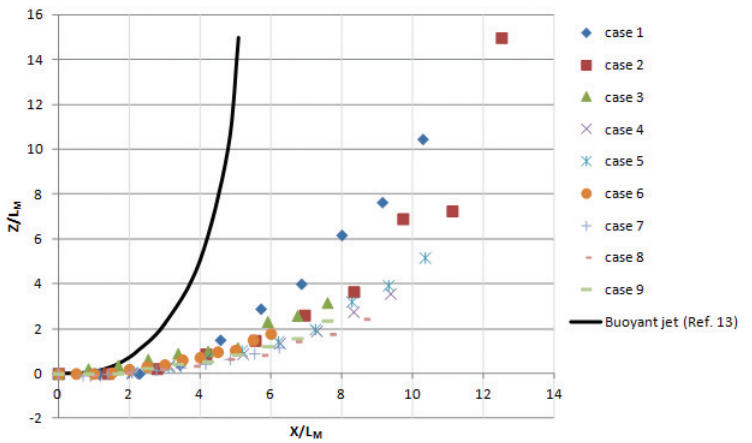

(a)

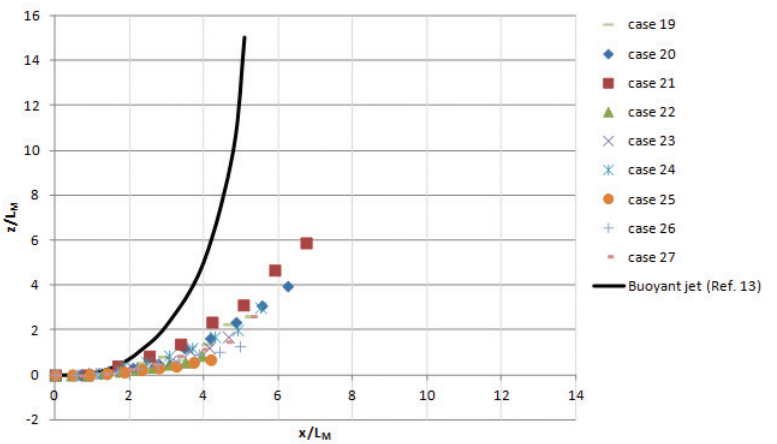

(b)

Figure 17. Trajectory of the flame provided in terms of momentum length, based on reacting Froude number for (a) propane and (b) ethylene. Results are compared to the integral formulation curve fit for a buoyant jet, (CORMIX, provided by Jirka in ref. 13).

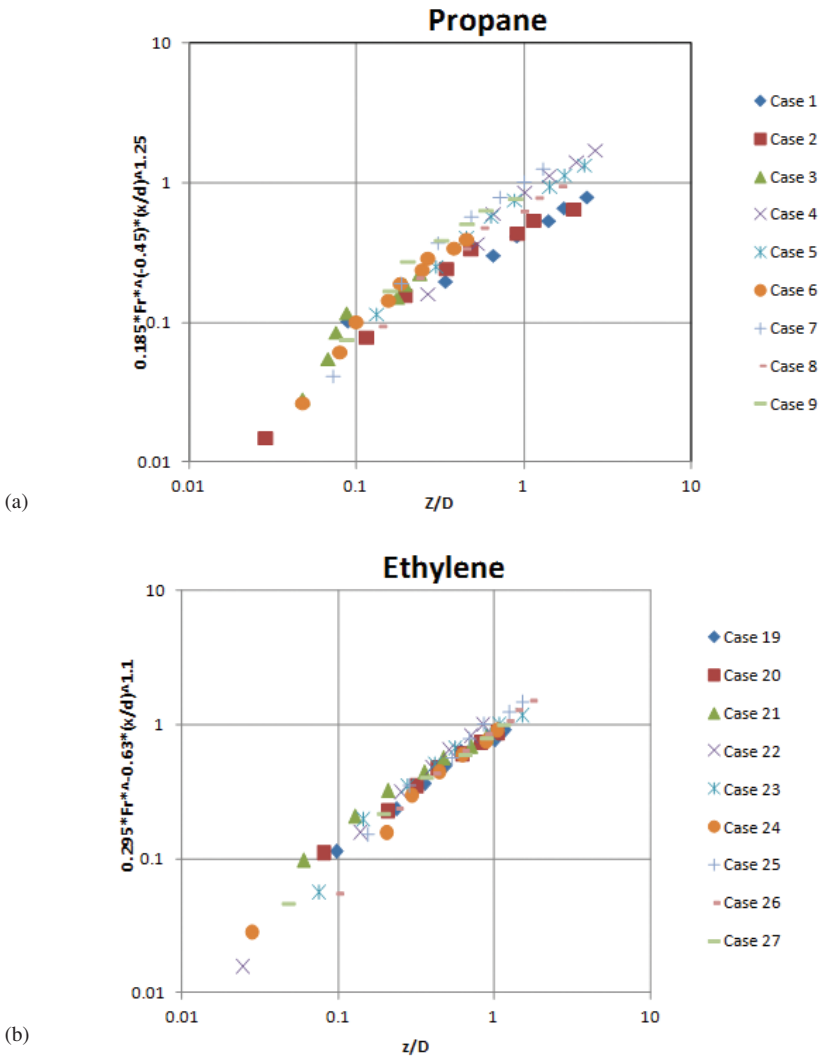

Figure 18. Comparison of raw data to empirical curve fits of trajectory for (a) propane and (b) ethylene.

fully for both fuel types. Further comparison of the plots of propane and ethylene suggest that the momentum-length-normalized trajectory for the ethylene diffusion flame is closer to that of a buoyant jet. This result is consistent with the fact that the density of unreacted propane is much higher than that of ethylene.

To provide additional utility for predicting the trajectory for the specific fuels tested, trajectory data for these experiments were empirically curve-fit using reacting Froude

number and jet diameter as normalization parameters. Although this approach is less satisfactory than one based on first principles, there is precedence in the literature for such empirical approaches due to their utility to applications related to combustion. For instance, Sato et al. developed a empirical correlation for length of a vertical diffusion flame based on a combination of Froude and Reynolds numbers [26]. The equations used to fit the data are given for propane and ethylene in Equations 5 and 6, respectively.

$$\text{Propane}: \quad \frac{z}{D} = 0.185 * \left(Fr^*\right)^{-0.45} * \left(\frac{x}{D}\right)^{1.25} \tag{5}$$

$$\text{Ethylene}: \quad \frac{z}{D} = 0.295 * \left(Fr^*\right)^{-0.63} * \left(\frac{x}{D}\right)^{1.1} \tag{6}$$

The curve fits capture the trajectory data over a range of Re from 300 to 1500 for propane and ethylene and a reacting Froude number range from 0.08 to 1.19 for propane and from 0.16 to 2.36 for ethylene. The data within this range is well characterized by this curve fit, as shown in Figure 18. As with any empirical formulation, care should be taken in extrapolating the expression outside the bounds of the experiment.

4. CONCLUSIONS

Characterization of combusting, horizontally issuing, buoyant jets was achieved through a series of PLIF and flame imaging experiments. The experiments encompassed two fuels, propane and ethylene with Reynolds numbers ranging from 300 to 1500. All resulting jet flames displayed characteristics consistent with jets with positive buoyancy. Even propane, which is denser than air turned upward due to the decreased density associated with the effects of combustion. Flame trajectory was measured with PLIF and checked against visualization data. Various jet diameters were used to enable the Reynolds number to be matched at different Froude numbers and vice versa. For a given gaseous fuel, the trajectory, by and large, collapsed with reacting Froude number based on a stoichiometric reaction. Variations in Reynolds number from 300 to 1500 only mildly influenced the overall shape of the trajectory.

One of the more interesting findings was the dramatic difference between the reaction zone on the top and the bottom mixing layer of the diffusion flame. In all cases, a substantially higher concentration of the combustion byproducts OH^- and PAH were observed developing on the top portion of the jet core. The OH^- occurred on the outermost portion of the mixing layer and initiated as a teardrop shape. The upper portion of the teardrop shape was observed only for measurements acquired very near the fuel jet exit, in part due to a rapid upward ascent of the high OH^- concentration region. By contrast, the development of the high PAH concentration region was manifested as a downward indentation on the upper portion of the jet cross-section. If one makes the plausible assumption that the region encompassed by the OH^- but absent

of either OH^- or PAH contained only unburned hydrocarbons, then it was clear that the last portion of core fuel remained near the lower edge, rather than in the center, of the jet. These attributes of a horizontally-issuing diffusion flame may yield insight into the behavior of fuel in a more general class of applications where buoyancy influences flame propagation and combustion rates.

Characterizing the flame trajectory by normalizing by the momentum length scale led to a reasonable outcome. The measured trajectories did not equate to renditions of that for a cold-flow buoyant jet found within the literature but rather were flatter, especially for propane — the more dense fuel. This result is consistent with the premise that the time required for reaction delayed the upward motion of the diffusion flame. These measurements provide a benchmark which will be useful as a more fundamental basis for the results is sought.

ACKNOWLEDGMENTS

The views expressed in this article are those of the authors and do not reflect the official policy or position of the United States Air Force, Department of Defense, or the U.S. Government. This work was a grant from the United States Air Force Office of Scientific Research, and the authors would like to thank contract monitor, Dr. Julian Tishkoff for his oversight of the project. The authors of this paper would also like to acknowledge Dr. Cam Carter of the Air Force Research Laboratory, Propulsion Directorate for assistance in interpreting the PLIF data. The authors would also like to thank Mr. John Hixenbaugh and Jay Anderson from the Air Force Institute of Technology for assisting with the experiment.

REFERENCES

[1] J. Zelina, J., R.T. Greenwood, D.T. Shouse, Operability and efficiency performance of Ultra-Compact, High Gravity Combustor Concepts, Paper GT2006-90119, Proceedings of 51st ASME International Gas Turbine and Aeroengine Congress and Exposition, May 2006.

[2] P.S. Kolhe, A.K. Agrawal, Role of buoyancy on instabilities and structure of transitional gas jet diffusion flames. *Flow Turbulence Combust*., 2007, 79, 343-360.

[3] I. Boxx, C. Heeger, R. Gordon, B. Bohm, M. Aigner, A. Driezler, W. Meier, Simultaneous three-component PIV/OH-PLIF measurements of a turbulent lifted, C_3H_8-Argon jet diffusion flame at 1.5 kHz repetition rate. *Proc. Comb. Inst*., 2009, 32, 905-912.

[4] A.A. Idicheria, I.G. Boxx, N.T. Clemens, Characteristics of turbulent nonpremixed jet flames under normal-and low-gravity conditions. *Combustion and Flame*, 2004, 138, 384-400.

[5] P.B. Sunderland, R.L. Axelbaum, D.L. Urban, B.H. Chao, S. Liu, Effects of structure and hydrodynamics on the sooting behavior of spherical microgravity diffusion flames. *Combustion and Flame*, 2003, 132, 25-33.

[6] H. Becker, D. Liang, Effect of burner orientation and ambient airflow on geometry of turbulent free diffusion flames. Eighteenth Symposium on Combustion, 1981, 1061-1071.

[7] J.P. Gore, C.Q. Jian, Analytical solution to the flame trajectory based on the analysis of 'Scaling of buoyant turbulent jet diffusion flames' by N. Peters and J. Gottgens'. *Combustion and Flame*, 1993, 93, 336-337.

[8] N. Peters, J. Gottgens, Scaling of Buoyant Turbulent Jet Diffusion Flames, *Combust. and Flame*, 1991, 85, 206-214.

[9] M.P. Escudier, Analysis and observations of inclined turbulent flame plumes. *Comb. Science and Tech.* 1975, 10, 163-171.

[10] T. Smith, C. Periasamy, B. Baird, S.R. Gollahalli, Trajectory and Characteristics of Buoyancy and Momentum Dominated Horizontal Jet Flames From Circular and Elliptic Burners. *J. Energy Resour. Technol.* 2006, 128, 300-310.

[11] K.H. Arakeri, D. Das, J. Srinivasan, Bifurcation in a buoyant horizontal laminar jet. *J. Fluid Mech.* 2000, 412, 61-73.

[12] M.F. Reeder, R.E. Huffman, R.D., Branam, K.D. Lebay, S.M. Meents, Mixing of gas-phase buoyant horizontal laminar jet measured with filtered Rayleigh scattering, *Exp. Fluids*, 2011, 50, 1455-1472.

[13] G. Jirka, Integral model for turbulent buoyant jets in unbounded stratified flows. Part I: single round jet. *Environ. Fluid Mech.*, 2004, 4, 1–56.

[14] J. Xiao, J.R. Travis, W. Breitung, Non-Boussinesq integral model for horizontal turbulent buoyant round jets. *Science and Technology of Nuclear Installations*, 2009, Article ID 862934,7 pages.

[15] F.P. Incropera, D.P. DeWitt, T.L. Bergman, S.A. Lavine, *Fundamentals of Heat and Mass Transfer*, 6th Edition, 740-741, John Wiley and Sons, Hoboken NJ, 2007.

[16] I. Glassman, *Combustion*, 2nd Edition, 465-471, Academic Press Inc, London, 1987.

[17] C.R. Shaddix, T.C. Williams, L.G. Blevins, R.W. Schefer, Flame structure of steady and pulsed sooting inverse jet diffusion flames, *Proc. Comb. Inst.*, 2005, 30, 1501-1508.

[18] S.Y.. Lee, S.R. Turns, R.J. Santoro, Measurements of soot, OH^-, and PAH concentrations in turbulent ethylene/air jet flames. *Combust. Flame* 2009, 156, 2264-2275.

[19] S.H. Won, W. Sun, Y. Ju, Kinetic effects of toluene blending on the extinction limit of n-decane diffusion flames. *Combust. Flame* 2010, 157, 411-420.

[20] H. Böhm, K. Kohse-Höinghaus, F. Lacas, C. Rolon, N. Darabiha, S. Candel, On PAH formation in strained counterflow diffusion flames," *Combust. and Flame* 2001, 124, 127-136.

[21] T.C. Williams, C.R. Shaddix, R. Schefer, P., Desgroux, The response of buoyant laminar diffusion flames to low-frequency forcing. *Combust. Flame*, 2007, 151, 676-684.

[22] M. Yamamoto, S. Duan, S. Senkan, The effect of strain rate on polycyclic aromatic hydrocarbon (PAH) formation in acetylene diffusion flames. *Combust. Flame,* 2007, 151, 532-541.

[23] E. Deri, A. Monavon, E. Studer, D. Abdo, I. Tkatschenko, Early development of the veil-shaped secondary flow in horizontal buoyant jets. *Phys. Fluids,* 2011, 23, 073604.

[24] J. Arakeri, D. Das, J.Srinivasan, Bifurcation in a buoyant horizontal laminar jet, *J. Fluid Mech.* 2000, 412, 61-73.

[25] J. Heffernen, *Characterization of Horizontally-Issuing Reacting Buoyant Jets*, M.S. Thesis Air Force Institute of Technology, Dept. Aeronautics and Astronautics, March 2011.

[26] H. Sato, K. Amagai, M. Arai, Diffusion Flames and Their Flickering Motions Related with Froude Numbers under Various Gravity Levels, *Comb. Flame*, 2000, 123, 107-118.